

http://pubs.acs.org/journal/aesccq Article

# Kinetics and Thermochemistry of Hydroxyacetonitrile (HOCH<sub>2</sub>CN) and Its Reaction with Hydroxyl Radical

Paul Marshall\* and James B. Burkholder



**Cite This:** ACS Earth Space Chem. 2024, 8, 1933–1941



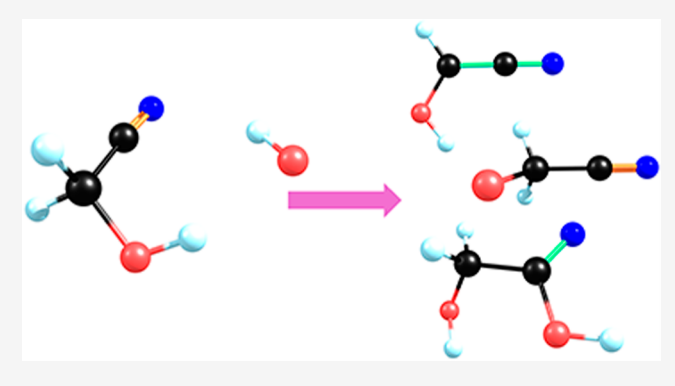
**ACCESS** 

III Metrics & More

Article Recommendations

Supporting Information

ABSTRACT: The potential energy surface for OH + HOCH<sub>2</sub>CN was investigated computationally with B2PLYP-D3/cc-pVTZ density functional theory for geometries and frequencies, and coupled-cluster theory with double, triple and perturbative quadruple excitations approximately extrapolated to the complete basis set limit for energies. The results were employed with canonical variational transition state (TS) theory and an Eckart tunneling model to obtain rate coefficients, k, for three channels, (1) H abstraction from the C–H bonds, (2) H abstraction from the O–H bond and (3) addition to the nitrile C atom. Over 220–450 K,  $k_1$ (T) = 2.07 × 10<sup>-13</sup> (T/298 K)<sup>2.264</sup> exp(+15 K/T) cm<sup>3</sup> molecule<sup>-1</sup> s<sup>-1</sup> and is the dominant pathway, accounting for ca. 85% of total reactivity at 298 K and 1 atm.  $k_2$ (T) = 5.16 × 10<sup>-15</sup>



 $(T/298 \text{ K})^{3.470} \exp(+440 \text{ K/T})$  and the high-pressure limit for channel 3,  $k_{3,\infty}(T)$ , was found to be temperature-independent with a value of  $2.2 \times 10^{-14} \text{ cm}^3$  molecule<sup>-1</sup> s<sup>-1</sup>. Consideration of the low-pressure limit and falloff indicates the high-pressure limit is the relevant quantity for atmospheric conditions. Intramolecular hydrogen bonding both stabilizes the TSs and makes them less flexible. The tropospheric lifetime of HOCH<sub>2</sub>CN with respect to reaction with OH is estimated to be ~45 days. Its major degradation product is predicted to be HC(O)CN, with minor contributions from HOC(O)CN and other species. Thermochemistry for HOCH<sub>2</sub>CN and these two products was obtained.

KEYWORDS: tropospheric chemistry, lifetime, wildfire, astrochemistry, transition state theory

## 1. INTRODUCTION

Biomass burning influences atmospheric composition, the climate and ecology and is the major atmospheric source of nitrile compounds. Emission of reactive nitrogen compounds, including nitrogen-containing volatile organic compounds (NVOCs), from wildfires impacts air quality and human health, and is a topic of current research.<sup>2</sup> Recent work in this laboratory has shown that 2-hydroxyacetonitrile (HOCH<sub>2</sub>CN, HAN), an isomer of methyl isocyanate, is emitted from wildfires.3 There is considerable information about the rotational spectrum, 4-6 however, little is known about the gas-phase thermochemistry, IR and UV spectroscopy or reactivity of HOCH2CN. A primary goal of the present work is to predict the reactivity of HOCH2CN with the hydroxyl radical under conditions relevant to the troposphere, estimate its atmospheric lifetime with respect to OH radical reactivity, and evaluate likely degradation products.

Here we investigate four OH + HAN reaction pathways computationally. There are two sites for H atom abstraction plus possible addition to either end of the CN group

$$HOCH_2CN + OH \rightarrow HOCHCN + H_2O$$
  
 $\Delta H_0 = -132.5 \text{ kJ mol}^{-1}$  (R1)

$$\rightarrow$$
 OCH<sub>2</sub>CN + H<sub>2</sub>O  $\Delta H_0 = -45.9 \text{ kJ mol}^{-1}$  (R2)

$$\rightarrow$$
HOCH<sub>2</sub>C(OH)N  $\Delta H_0 = -111.7 \text{ kJ mol}^{-1}$  (R3)

$$\rightarrow$$
HOCH<sub>2</sub>CNOH  $\Delta H_0 = + 78.7 \text{ kJmol}^{-1}$  (R4)

where the  $\Delta H_0$  values were obtained in the present work. The uncertainties are  $\pm 1.5$  kJ mol $^{-1}$  (see Section 3.1). The thermochemistry of HAN has not been measured and the first part of this work was to derive an accurate heat of formation, to allow assessment of feasible reaction pathways and dissociation equilibria. The central thrust of the study was to obtain temperature-dependent rate coefficients relevant to atmospheric chemistry, for which there are no prior experimental or theoretical data. These were used to assess the tropospheric lifetime. To predict the reaction rate

Received: June 17, 2024 Revised: August 12, 2024 Accepted: August 13, 2024 Published: August 20, 2024





coefficients, canonical variational transition state (TS) theory was applied with information about the potential energy surfaces for reactions (R1-R4) obtained at levels of theory that approximate coupled cluster theory through quadruple excitations at the complete basis set limit, along with an accounting for vibrational and torsional anharmonicity in the normal modes.

We also discuss the potential atmospheric fate of HAN and its likely degradation products such as formyl cyanide, HC(O)CN, and cyanoformic acid, HOC(O)CN. These three species are also relevant to astrochemistry, where compounds containing a CN group are of interest as prebiotic precursors to amino acids and nucleobases, implicated in the origins of life. This has motivated detailed studies of the rotational energy levels of HOCH<sub>2</sub>CN to assist radio astronomy detection. HC(O)CN was isolated in the laboratory in 1992 and detected in a star-forming region in 2008. HAN was similarly detected in 2019. In this context, Zhao et al. have analyzed some of its reactions computationally, with a focus on H atom loss or its reverse and emphasizing surface-adsorbed species, but no gas-phase kinetics data are available.

#### 2. METHODOLOGY

Geometries of bound minima and TSs on the potential energy surface for OH + HOCH2CN were characterized with the B2PLYP-D3/cc-pVTZ level of density functional theory (DFT). 12-14 This was chosen because it "provides [coupled cluster with single, double and perturbational triple excitations] CCSD(T) quality geometries and frequencies" at low computational cost. 15 The stability of the wave function at the stationary points was verified, and the intrinsic reaction coordinates (IRC) were followed to confirm the species connected by the TSs. Fundamental vibrational frequencies were evaluated by scaling the harmonic frequencies  $\omega$  by  $1.045-0.00851 \omega^{0.292}$  as proposed by Elliott et al. 15 for H/C/ O species. Compared to a large training set obtained via anharmonic vibrational second-order perturbation (VPT2) analysis, they found a rms deviation of 13 cm<sup>-1</sup> per normal mode. As a check on application of this scaling to a nitrogencontaining molecule similar to HAN (and likewise outside the H/C/O training set) we examined CH<sub>3</sub>CN. Compared to the experimental fundamental frequencies, 16 DFT scaled as above yielded a rms deviation of 18 cm<sup>-1</sup> per mode. For zero-point vibrational energy (ZPVE), a constant scale factor was applied so that ZPVE =  $0.9863 \times 1/2 \Sigma \omega$ , which Elliott et al. found to have a rms error of 0.7 kJ mol<sup>-1</sup> per molecule compared to VPT2 results for their training set. 15 For our test case of CH<sub>3</sub>CN, combination of DFT with VPT2 reveals an error of  $-0.4 \text{ kJ mol}^{-1}$  in the simple scaling approach for ZPVE.

Single-point electronic energies were obtained with coupled cluster theory extrapolated to the complete basis set limit,  $E_{CBS}$ , using energies at  $CCSD(T)^{17}$  with the cc-pVTZ and cc-pVQZ basis sets, <sup>14</sup> denoted as  $E_n$  with n=3 and 4, respectively. The  $T_1$  diagnostic <sup>18</sup> was monitored to check for excessive multireference character which would make the single-reference methodology unreliable.  $E_n$  is the sum of the Hartree–Fock and correlation energies,  $E^{HF} + E^{corr}$ , which were extrapolated separately to their CBS limits as follows <sup>19</sup>

$$E_{\rm CBS}^{\rm HF} = E_n^{\rm HF} - A \exp(-\alpha n^{1/2}) \tag{1}$$

where  $\alpha$  is fixed at 5.46 and A is a species-specific parameter, and

$$E_{\rm CBS}^{\rm corr} = (3^{\beta} E_3^{\rm corr} - 4^{\beta} E_4^{\rm corr}) / (3^{\beta} - 4^{\beta}) \tag{2}$$

where  $\beta$  = 3.05, and then added. All the quantum calculations were made with the Gaussian 16 program, <sup>20</sup> except for a higher-level correction for electron correlation to include exact triple and perturbative quadruple excitation terms, defined here as

$$E_{HL} = E(CCSD(T)/cc-pVDZ) - E(CCSDT(Q)/cc -pVDZ)$$
(3)

This last step was evaluated with the MRCC program<sup>21</sup> integrated with Cfour.  $^{22}$   $E_{\rm CBS}$  for the OH radical was corrected down by 0.83 kJ mol<sup>-1</sup> to account for its spin—orbit splitting.  $^{16}$   $E_{\rm CBS}$  for all species were then modified by adding the ZPVE to obtain the final energy  $E_{\rm total}$  as

$$E_{\text{total}} = E_{\text{CBS}}^{\text{HF}} + E_{\text{CBS}}^{\text{corr}} + E_{\text{HL}} + \text{ZPVE}$$
 (4)

Differences in  $E_{\rm total}$  between reactants and TS or products correspond to enthalpy changes at 0 K,  $\Delta H_0$ . For loose complexes of radicals with closed shell molecules, convergence difficulties interfered with computation of  $E_{\rm HL}$  and so this term was left out of their  $\Delta H_0$  calculations. This should cause minimal error because valence forces are minor for these longrange systems. <sup>23</sup>

The thermochemistry of HAN was assessed by computation of  $\Delta H_0$  for a hypohomodesmotic working reaction<sup>24</sup> which conserves the number and type of bonds and the hybridization of the carbon atoms

$$HOCH_2CN + C_2H_6 \rightarrow HOCH_2CH_3 + CH_3CN$$
 (R5)

This process is chosen to cancel computational errors. The enthalpies of formation of ethane, ethanol and acetonitrile are accurately known from the Active Thermochemical Tables (ATcT), the source for all ancillary thermochemistry used here unless otherwise noted. Given the computed reaction enthalpy for reaction (R5),  $\Delta_{\rm f}H_0({\rm HAN})$  is derived. The fundamental frequencies were used to evaluate the thermal correction  $H_{298}-H_0$  for HAN and, together with the  $H_{298}-H_0$  for the elements in their standard states,  $^{26}$   $\Delta_{\rm f}H_{298}({\rm HAN})$  is obtained. Possible atmospheric degradation products of HAN (see later) are suggested to be HC(O)CN and HOC(O)CN, and they were analyzed via analogous working reactions

$$HC(O)CN + C_2H_6 \rightarrow CH_3CHO + CH_3CN$$
 (R6)

$$HOC(O)CN + C_2H_6 \rightarrow CH_3C(O)OH + CH_3CN$$
(R7)

Rate coefficients k were calculated via canonical variational TS theory, CVTST,<sup>27</sup> as the minimum of k with respect to s, the distance of the TS along the reaction coordinate from the saddle point

$$k = \min_{s} \kappa \frac{k_{\rm B}T}{h} \frac{m_{\rm TS}}{m_{\rm reactant}} \frac{Q_{\rm TS}}{Q_{\rm OH}Q_{\rm HAN}} \exp\left(-\frac{E_0}{RT}\right) \tag{5}$$

where  $E_0$  is the 0 K energy of the TS relative to reactants,  $E_{\rm total}({\rm TS}) - E_{\rm total}({\rm OH}) - E_{\rm total}({\rm HAN})$ .  $E_{\rm total}({\rm TS})$  varies with its location. m is the number of optical isomers that do not interconvert via low-barrier internal rotations. Molecular partition functions Q were based on the harmonic oscillator-

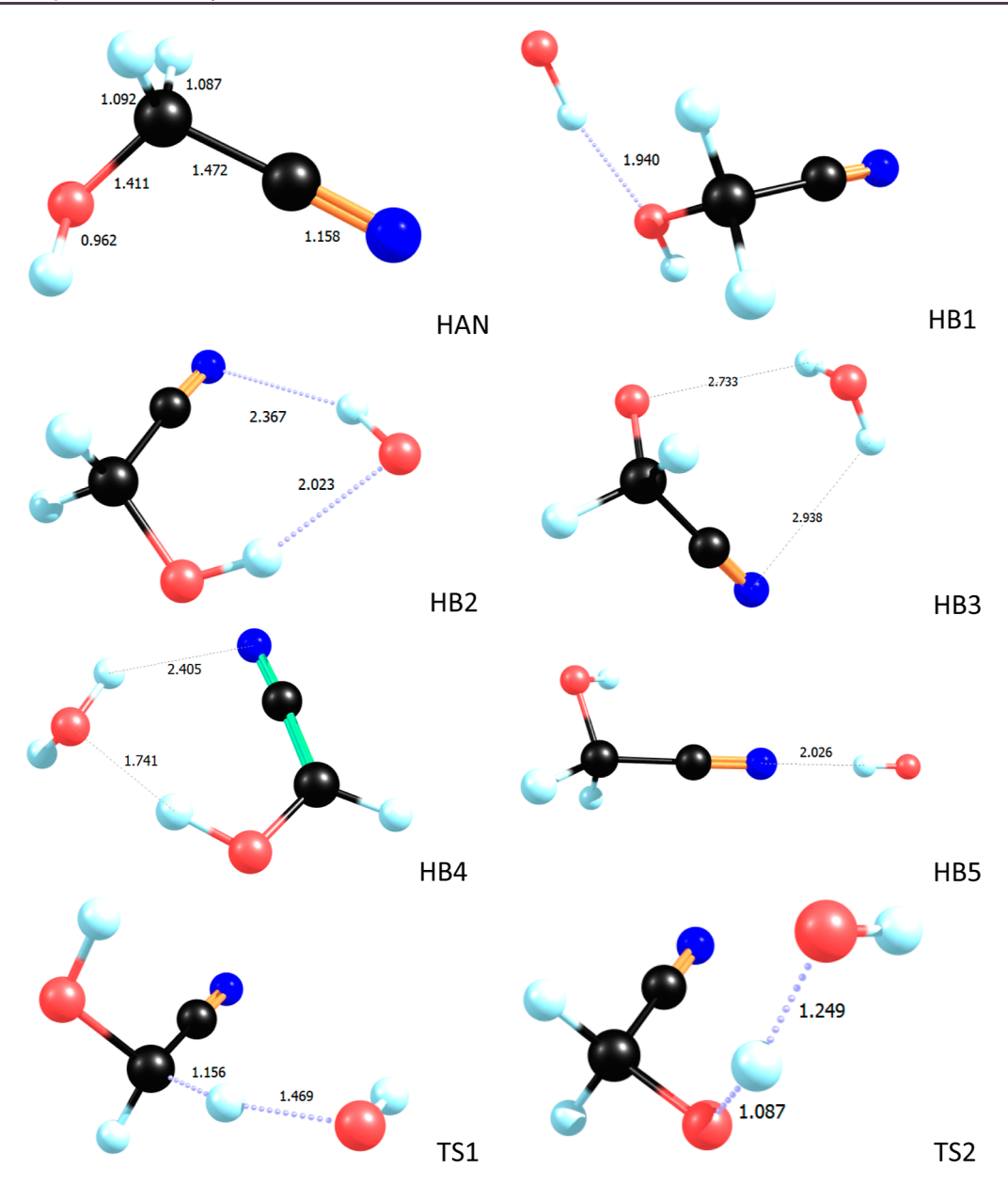


Figure 1. Structures of reactants, bound complexes, TSs and products for the reactions of hydroxyl with hydroxyacetonitrile from B2PLYP-D3/cc-pVTZ DFT. Selected bond lengths are shown in units of  $10^{-10}$  m. Atoms are denoted as oxygen (red), carbon (black), nitrogen (blue) and hydrogen (pale blue). A color version of this figure is available in the online version.

rigid rotor model using the scaled fundamental frequencies and the moments of inertia obtained from DFT, and include rotational symmetry factors  $\sigma$ . Low-barrier torsions, such as the hindered rotation of OH in HAN which connects the most stable gauche structure with a higher energy trans conformer, were treated as separable one-dimensional modes. For these modes, the torsional potential was evaluated over the  $2\pi$  range of torsion angle  $\varphi$  with B2PLYP-D3/cc-pVTZ theory in 32 steps, and a discrete Fourier Transform was applied to express the potential as a sum of sine and cosine components of  $\varphi$  through  $6\varphi$ . This scan automatically accounts for the number of optical isomers along these paths. The hindered rotor partition function was obtained via the energy levels of the torsional potential as implemented in the Multiwell program. <sup>28</sup>

The highest value of  $E_0$  as a function of s, the distance along the mass-weighted IRC away from s=0 at the DFT saddle point, along with the neighboring points on either side, define

an inverted parabola. This yields the curvature of the vibrationally adiabatic ground-state (VAG) potential and, via the method of Coote et al.,<sup>29</sup> the imaginary frequency for motion along the IRC. In turn, this parameter, along with the forward and reverse barrier heights  $V_{\rm f}$  and  $V_{\rm r}$  at the local maximum of the VAG, allows the transmission correction factor  $\kappa$  for quantum mechanical tunneling to be evaluated with a simple one-dimensional Eckart model, based on a Boltzmann distribution of energy levels in the reactants. These Q and  $\kappa$  calculations were carried out with the Multiwell program.<sup>28</sup> To summarize, (i) anharmonicity in regular vibrations is accounted for by scaling, (ii) torsional anharmonicity is accounted for by evaluation of 1-D torsional potentials and their associated eigenvalues, which also (iii) incorporates different conformations that can interchange via the low-barrier torsions, while (iv) multistructural effects from different conformations that cannot interconvert via such

internal rotations, for example certain optical isomers, are accounted for with a separate factor m. Together with external rotational symmetry numbers  $\sigma$  (actually included within Q for overall rotation), the ratio  $m_{\rm TS}$   $\sigma_{\rm reactant}/(m_{\rm reactant}$   $\sigma_{\rm TS})$  is a reaction path degeneracy that multiplies the rate coefficient. Because  $\sigma$  (which is 1 for the present cases) is already included within Q for overall rotation, only the factor  $m_{\rm TS}/m_{\rm reactant}$  appears explicitly in eq 5.

Variational effects were evaluated by stepping along the IRC away from the saddle point of the VAG, and geometries at positive and negative s values were characterized with steps of 0.07, 0.16, and 0.05 amu bohr<sup>1/2</sup> for reactions (R1–R3), respectively, as trial locations for the TS. At each location, motion along the IRC was projected out and frequencies were scaled as before.  $E_{\text{total}}(\text{TS})$  was reevaluated at each of these locations, hence modified  $E_0$  values, with the assumption that  $E_{\text{HL}}$  was unchanged from the value at s=0 for small displacements. Along with the modified moments of inertia, scaled modified frequencies were used to calculate  $Q_{\text{TS}}$  and hence k as a function of s. At each temperature, the IRC point that minimized k together with the neighboring points, defined a quadratic function for k(s) used to interpolate k (by 1–10%) to our best estimate of its minimum value.

The inherently pressure-dependent kinetics for the addition reaction (R2) were predicted via Troe's unimolecular formalism.<sup>30</sup> Equation 5 yielded its high-pressure limit, and the low-pressure limit was predicted via the Statistical Adiabatic Channel Model detailed by Troe.<sup>30</sup> Atmospheric conditions were explored by interpolation between these limits using the simplified falloff relation employed by Burkholder et al.<sup>31</sup>

# 3. RESULTS AND DISCUSSION

**3.1. Thermochemistry.** Structures of the reactants, intermediates, TSs and products for (R1-R4) are shown in Figures 1 and 2, and their Cartesian coordinates are provided in Table S1 of the Supporting Information. As expected, for gauche HAN the DFT bond lengths are similar to those from the explicitly correlated coupled cluster calculations (CCSD-(T)-F12/aug-cc-pVTZ) made by Dalbouha et al., with mean and rms differences of 0.001 and 0.003 in units of 10<sup>-10</sup> m, respectively. Table S2 lists the initial computed harmonic frequencies before scaling, and Figure S1 shows the torsional potentials for those modes treated as hindered rotors. To date, the gas-phase infrared spectrum of HAN has not been published, although it has been studied in the liquid state<sup>32</sup> and in a frozen matrix. 33,34 We also summarize our predicted fundamental vibrational frequencies in Table S2, to assist future gas-phase identification of HAN.

Table S3 lists the results of the single-point energy calculations. The  $T_1$  values are below the general thresholds of  $T_1 < 0.044$  for radicals and  $T_1 < 0.02$  for closed-shell species, which indicates that single-reference coupled-cluster theory is valid. Via the working reaction (R5), we obtain the enthalpy of formation of HAN at 0 and 298 K to be -43.37 and -52.17 kJ mol $^{-1}$ , respectively. The ATcT uncertainties in the three reference values propagated in quadrature yield  $\pm 0.33$  kJ mol $^{-1}$ . We expect significant cancellation of any residual errors in  $E_{\rm total}$ . As a check, we considered an intentionally inferior isogyric working reaction

$$HOCH_2CN + 2H_2 \rightarrow H_2O + CH_4 + HCN$$
 (R8)

that yields  $\Delta_t H_0(\text{HAN}) = -43.55 \text{ kJ} \text{ mol}^{-1}$ , where uncertainties in the reference compounds together contribute

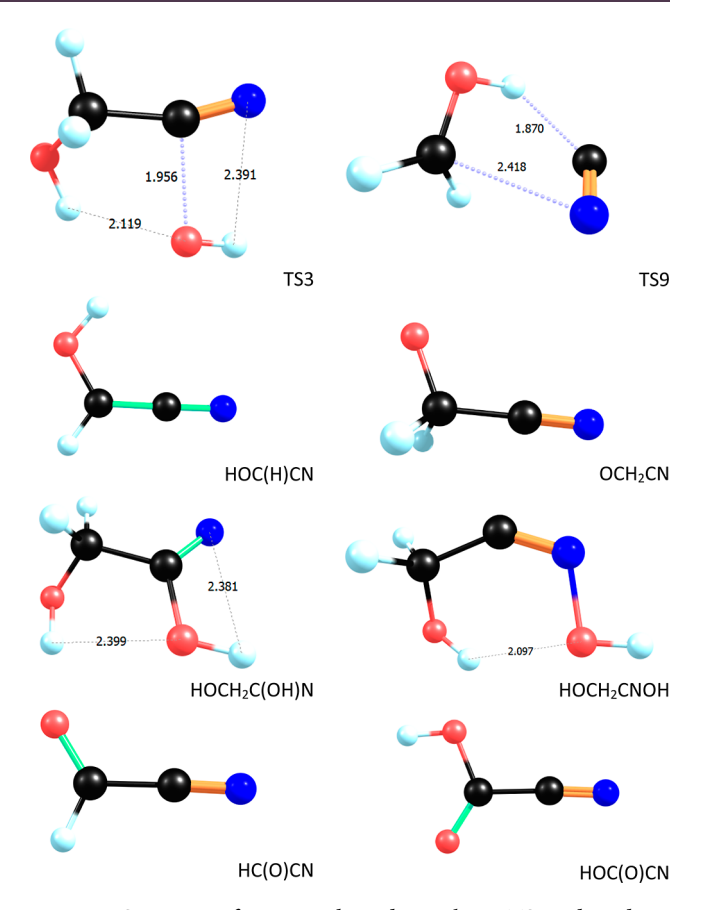


**Figure 2.** Structures of reactants, bound complexes, TSs and products for the reactions of hydroxyl with hydroxyacetonitrile from B2PLYP-D3/cc-pVTZ DFT. Selected bond lengths are shown in units of  $10^{-10}$  m. Atoms are denoted as oxygen (red), carbon (black), nitrogen (blue) and hydrogen (pale blue). A color version of this figure is available in the online version.

 $\pm 0.10~{\rm kJ~mol^{-1}}$ . The close accord of  $\sim 0.2~{\rm kJ~mol^{-1}}$  between the two approaches, where the second benefits from less error cancellation, is consistent with a conservative uncertainty of around 0.5 kJ mol<sup>-1</sup> for the hypohomodesmotic working reactions combined with our  $E_{\rm total}$  formalism. Combined in quadrature with the rms ZPVE uncertainty of 0.7 kJ mol<sup>-1</sup> for each species leads to a final uncertainty of  $\sim 1.5~{\rm kJ~mol^{-1}}$  ( $1\sigma$ ). For HAN thermochemistry there are no prior experiments or computations for comparison.

Substitution of  $E_{\text{total}}$  values into (R1-R4) yields the  $\Delta H_0$ values shown in the Introduction. A first step in rationalization of the reactivity of HAN is to consider the strengths of the breaking or forming bonds. In two related molecules, acetonitrile and methanol, the C-H bond dissociation enthalpy at 0 K (BDE) is lowered by about 36 kJ mol<sup>-1</sup> compared to that in methane, from 432.5 kJ mol<sup>-1</sup> in CH<sub>4</sub> to 397.7 kJ mol<sup>-1</sup> in CH<sub>3</sub>CN and 395.7 kJ mol<sup>-1</sup> in CH<sub>3</sub>OH. This may reflect stabilization of the resulting substituted methyl radicals by  $\pi$  electron donation from the OH or CN group toward the half occupied, electron deficient p orbital in the radical. Both groups together exhibit an additive effect, with a computed C-H BDE in HOCH<sub>2</sub>CN of 361.8 kJ mol<sup>-1</sup> i.e., lowered by a further ca. 35 kJ mol<sup>-1</sup>. One might therefore expect C-H abstraction kinetics in HAN to be more favorable than in the simpler analogs. For the O-H BDE, computation yields 446.4 kJ mol<sup>-1</sup> in HAN, 11 kJ mol<sup>-1</sup> higher than the

435.0 kJ mol<sup>-1</sup> found in methanol. OH can add to the C atom of the nitrile group in HAN, pathway (R3), with a computed C–O BDE in the product HOCH<sub>2</sub>(OH)N radical of 110 kJ mol<sup>-1</sup> at 0 K. For the analogous radical CH<sub>3</sub>C(OH)N formed from acetonitrile, our calculations yield 99 kJ mol<sup>-1</sup>. Thus, the addition product is slightly more strongly bound for HAN vs CH<sub>3</sub>CN and would be stable at ambient conditions. Addition of OH to the N atom in HAN is significantly endothermic, with a computed  $\Delta H_0 = +79$  kJ mol<sup>-1</sup>, so reaction (R4) will be both thermodynamically unfavorable and negligibly slow under atmospheric conditions, and therefore it is not considered further.

HAN can dissociate via a molecular channel

$$HOCH_2CN \rightarrow CH_2O + HCN$$
 (R9)

and the extent of dissociation in the gas-phase bears on the possible observation of HAN and its fate. The  $\Delta_{\rm f}H_{298}$  (HAN) together with  $\Delta_{\rm f}H_{298}$  of CH<sub>2</sub>O and HCN yield the enthalpy change for reaction in the gas-phase,  $\Delta H_{298} = +72.2$  kJ mol<sup>-1</sup>. We compute the entropy S<sub>298</sub> and C<sub>p,298</sub> for HAN as 295.2 and 67.9 J K<sup>-1</sup> mol<sup>-1</sup> and, combined with the entropies of the products, <sup>26</sup> this implies  $\Delta G^{\circ}_{298} = +34.8$  kJ mol<sup>-1</sup> when all species are present at partial pressures of 1 bar =  $10^5$  Pa. At 298 K the equilibrium constant is  $K_p = 8 \times 10^{-7}$  (standard state 1 bar) or  $K_c = 2 \times 10^{13}$  (standard state 1 molecules cm<sup>-3</sup>). Dissociation of HAN becomes more favorable as its partial pressure decreases, and for example starting with pure HAN at pressures of 10 mbar and 10 ppb, we predict degrees of dissociation of 0.009 and 0.99, respectively, at thermal equilibrium. Trace partial pressures of HAN are therefore thermodynamically unstable.

**3.2.** Kinetics of Hydroxyl Radical Reactions with Hydroxyacetonitrile. The relative 0 K enthalpies of OH + HAN, TSs and products (derived from relative  $E_{\text{total}}$  values listed in Table S3) for (R1–R3) are summarized in Table 1

Table 1. Relative Enthalpies of Stationary Points on the OH + HAN Potential Energy Surface at 0 K

species	enthalpy relative to reactants <sup>a</sup> /kJ mol <sup>-1</sup>
OH + HOCH <sub>2</sub> CN	0
HB1	-12.53
HB2	-22.21
TS1	4.85
TS2	12.19
TS3	0.99
HB3	-59.56
$H_2O + OCH_2CN$	-45.93
HOCH <sub>2</sub> C(OH)N	-111.67
HB4	-168.63
$H_2O + HOC(H)CN$	-132.54
$^a$ 1 $\sigma$ uncertainty of 1.5 kJ mo	$1^{-1}$ .

and plotted on a potential energy diagram in Figure 3, along with hydrogen-bonded complexes in the entrance and exit channels. The local maxima in the  $E_{\rm total}$  energies, which include ZPVE, along the IRC are close to the DFT saddle point that defines s=0. With these s values for reactions (R1–R3) equal to -0.095, 0.062, and 0.025 bohr amu<sup>1/2</sup>, respectively, it may be seen that DFT yields a close estimate of the geometry of the saddle point of the high-level VAG. At temperatures T>0, changes in the partition functions along the IRC further—slightly—shift the position of the variational TS (i.e., the s value

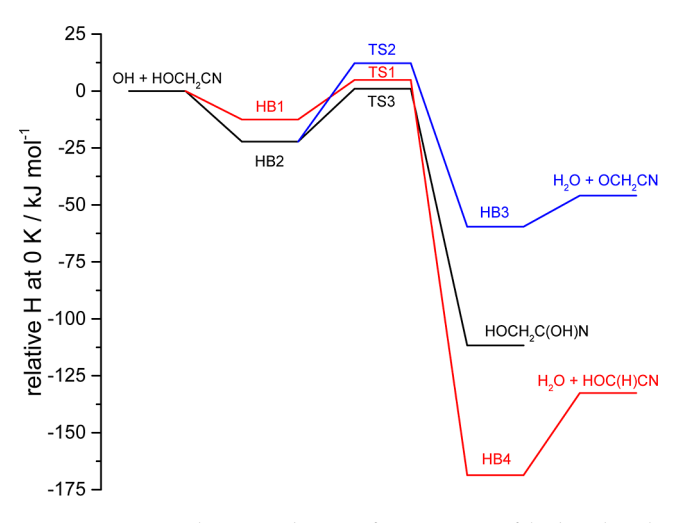


**Figure 3.** Potential energy diagram for reactions of hydroxyl with hydroxyacetonitrile based on approximate CCSDT(Q)/CBS results plus ZPVE (see text), showing the pathways for R1 (red), R2 (blue) and R3 (black). A color version of this figure is available in the online version.

where locating the TS minimizes  $k_i(T)$ ). The factors by which the variational analysis reduces  $k_i(450 \text{ K})$  compared to using simple TST at s=0 for i=1-3 are 1.14, 1.33 and 1.08, respectively, and decrease to 1.02, 1.03, and 1.01 at 220 K. Thus, variational effects are not large for our conditions of interest. The imaginary frequencies  $v_i$  for motion along the reaction coordinate evaluated from the curvature of the VAG potentials at their maxima for the three reactions are 944i, 2188i and 532i cm<sup>-1</sup>, respectively. This parameter reflects the narrowness of the barrier, so higher values imply more tunneling for a given barrier height. Because of the strongly nonlinear dependence of the tunneling correction factor  $\kappa$  of eq 5 on  $v_i$ , tunneling is much more important for abstraction of H from the hydroxyl group than for the other pathways.

The CVTST kinetics results for reactions (R1-R3) are plotted in Arrhenius format in Figure 4. The greatest rate coefficient is for (R1), whose rate expression is provided in Table 2.

A simple Arrhenius fit of  $k_1$  over this same temperature range yields a preexponential A factor of about  $2\times 10^{-12}$  cm<sup>3</sup> molecule<sup>-1</sup> s<sup>-1</sup>, in line with typical A factors for H abstraction by the OH radical. The alternative abstraction path (R2) rate coefficient is an order of magnitude lower (Table 2). Despite a barrier 7.3 kJ mol<sup>-1</sup> higher than for (R1), the temperature dependence is similar. Partly this reflects the increasing influence of quantum mechanical tunneling with decreasing temperature. At 298 K the factor  $\kappa$  of eq 5 is 1.6 for  $k_1$  and 8.8 for  $k_2$ , while at 220 K the values are 2.4 and 46, respectively.

For channel R3, addition of OH to the C atom of the nitrile group to yield the  $HOCH_2C(OH)N$  radical, the CVTST analysis yields the high-pressure limit  $k_{3,\infty}$ , which is similar to  $k_2(298 \text{ K})$ . The barrier is small,  $\sim 1 \text{ kJ mol}^{-1}$ , hence the negligible temperature-dependence of  $k_{3,\infty}(T)$ , which is constant to within 5% at  $2.2 \times 10^{-14}$  cm³ molecule $^{-1}$  s $^{-1}$ , and the role of tunneling is negligible. The pre-exponential factor is lowered in the moderately tight TS3, where the barriers to rotation of the hydroxyl group in HAN and of the incoming hydroxyl group are high, at 26 and 41 kJ mol $^{-1}$ , respectively. This reflects dipole—dipole attraction between the OH and CN groups that holds them nearly parallel (see Figure

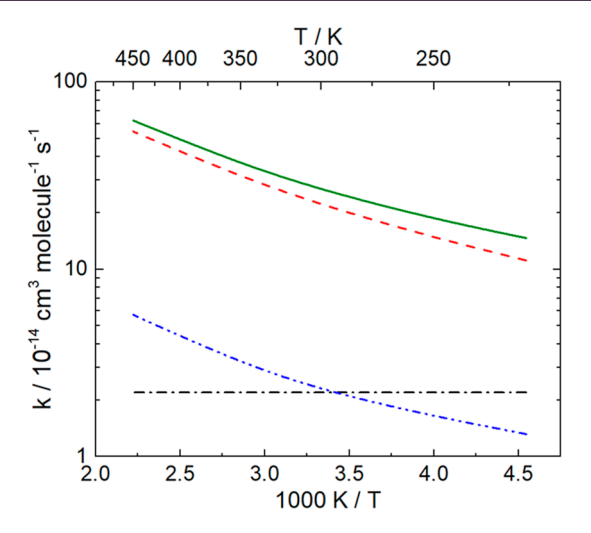


Figure 4. Arrhenius plot of computed rate coefficients for reactions of hydroxyl with hydroxyacetonitrile, showing the pathways for R1 (red dashed line), R2 (blue dash dot dot line), R3 (black dash dot line) and total (green solid line). A color version of this figure is available in the online version.

1), while this and a hydrogen-bonding interaction with the hydroxyl group stabilize TS3 and contribute to the low barrier. The pressure dependence of  $k_3$  was predicted via Troe's SACM model, with a threshold energy of 112.7 kJ mol<sup>-1</sup> for the dissociation of HOCH<sub>2</sub>C(OH)N back to OH + HAN. A typical and constant average energy transferred in collisions with N<sub>2</sub> bath gas of  $\langle \Delta E \rangle = -4$  kJ mol<sup>-1</sup> was assumed, which at 298 K implies a collisional efficiency of  $\beta_c = 0.44$ .  $\beta_c$  varied from 0.53 at 220 K to 0.37 at 450 K. The low-pressure limit  $k_{3,0}(220-450 \text{ K})$  was estimated as  $4.0 \times 10^{-29} (T/298 \text{ K})^{-3.42}$ cm<sup>6</sup> molecule<sup>-2</sup> s<sup>-1</sup>. Interpolation of the falloff curve for 298 K reveals that the effective second-order rate coefficient is within 10% of the high-pressure limit when the bath gas pressure exceeds 3 mbar, so falloff can be neglected under tropospheric conditions. Given our computed equilibrium constant for (R3) of  $K_c = 6.8 \times 10^{-28} \exp(-13,800 \text{ K/T}) \text{ cm}^3 \text{ molecule}^{-1}$ , and the above  $k_{2,\infty}(T)$  expression, we can deduce that at the highpressure limit the lifetime of the HOCH2C(OH)N adduct with respect to dissociation is of the order of a year at 298 K, but drops to the order of a second at 450 K. Thus, the adduct is nonreactive with respect to OH loss at ambient temperature, although of course the HOCH<sub>2</sub>C(OH)N adduct is a labile radical.

**3.3.** Complex Formation with Hydroxyl Radical. A feature of the abstraction reaction paths is the formation of bound complexes, with reactant complexes, HB1 and HB2, before the TSs and postbarrier complexes between the products, HB3 and HB4, see Figures 1 and 3. As discussed below, these complexes do not significantly affect the kinetics under tropospheric conditions.

HB1 is bound by a 12.5 kJ mol $^{-1}$  interaction (at 0 K, including ZPVE, relative to reactants) between the H atom of the hydroxyl radical and the O of HAN, with a short hydrogen bond length shown on Figure 1 of 1.94  $\times$  10 $^{-10}$  m and where the O atom of the hydroxyl could go on to attack a C-H bond via reaction(R1). HB2 is bound by two interactions whose combined strength is 22.2 kJ mol $^{-1}$ . The H atom of the hydroxyl group is 2.37  $\times$  10 $^{-10}$  m from the N atom of HAN and the hydroxyl's O atom is 2.02  $\times$  10 $^{-10}$  m from the H atom of HAN's alcohol group. In HB2 the hydroxyl radical is positioned for H-abstraction from the OH group of HAN via reaction (R2). There is a further HB5 complex with OH along the NCC axis of HAN with an N-H separation of 2.03  $\times$  10 $^{-10}$  m and bound by 15.7 kJ mol $^{-1}$ , but this is not clearly part of a further reaction path.

The kinetics calculations via eq 5 correspond to the lowpressure limit, where bound vibrational energy levels of prereactive complexes are unpopulated and do not contribute to the rate coefficient. If collisional stabilization populated lower energy levels of HB1 and HB2, and if these levels tunneled through the barriers at TS1 and TS2, then in principle these levels could contribute to overall reaction via tunneling to the products. Under these conditions pathway (R2) would be favored because of the narrower barrier (larger v<sub>i</sub>) permitting enhanced tunneling. At low enough temperatures, the tunneling rate of a prereactive complex may become so fast that the reaction bottleneck becomes initial capture of OH to form the prereactive complex. Typical capture rate coefficients are of the order of  $10^{-10} - 10^{-9}$  cm<sup>3</sup> molecule<sup>-1</sup> s<sup>-1</sup> so the consequence is a major increase in the observed rate coefficient at low temperatures, often occurring at around 50-150 K depending on the reactant.<sup>36</sup>

As a check on whether this effect could be significant under tropospheric conditions, we focus on HB2 because it is more strongly bound than HB1 and tunneling is favored for (R2). With an assumed A factor for HB2 dissociation back to reactants of  $10^{15}$  s<sup>-1</sup> and a threshold of 22 kJ mol<sup>-1</sup>, HB2 molecules formed at 220 K with an energy above OH + HAN of 3/2 RT (the average kinetic energy), we use the Inverse Laplace Transform method<sup>37</sup> to estimate the microcanonical k(E) for dissociation as  $8 \times 10^{11}$  s<sup>-1</sup>. Collisional stabilization is slower than this at pressures of 1 atm or less, so HB1 and HB2 have negligible impacts under atmospheric conditions.

Based on the broad similarity between properties of HB2 and TS2 and the analogous complex and TS for H abstraction from the hydroxyl group of methanol, it is reasonable to expect  $k_2$  to increase significantly at similar temperatures, i.e., at ca. 150–200 K, and to approach the OH + HAN capture rate coefficient  $k_{\rm cap}$  at around 50–100 K. For capture dominated by dipole–dipole interactions we apply the longrange variational TS theory of Georgievskii and Klippenstein to obtain  $k_{\rm cap} = 5.7 \times 10^{-10} \ (298 \ {\rm K/T})^{1/6} \ {\rm cm}^3 \ {\rm molecule}^{-1} \ {\rm s}^{-1}$ . These extremely low temperatures are outside the realm of

Table 2. Summary of Computed Rate Coefficients for OH + HOCH<sub>2</sub>CN

reaction products	$k(298 \text{ K})/\text{cm}^3 \text{ molecule}^{-1} \text{ s}^{-1}$	$k(220-450 \text{ K})/\text{cm}^3 \text{ molecule}^{-1} \text{ s}^{-1}$
$HOCHCN + H_2O(R1)$	$2.2 \times 10^{-13}$	$2.07 \times 10^{-13} (T/298 \text{ K})^{2.264} \exp(+15 \text{ K/T})$
$OCH_2CN + H_2O (R2)$	$2.3 \times 10^{-14}$	$5.16 \times 10^{-15} (T/298 \text{ K})^{3.470} \exp(+440 \text{ K/T})$
$HOCH_2C(OH)N$ (R3)	$2.2 \times 10^{-14}$	$2.2 \times 10^{-14}$
overall	$2.6 \times 10^{-13}$	$8.2 \times 10^{-12} \exp[(1.12 \times 10^5 \text{ K}^2/\text{T} - 1430 \text{ K})/\text{T}]$

atmospheric chemistry, although relevant to interstellar chemistry, and were not pursued further in the present work.

**3.4.** Implications for Atmospheric Chemistry. The sum of rate coefficients for pathways (R1–R3) at 298 K gives an effective rate coefficient of  $2.6 \times 10^{-13}$  cm³ molecule<sup>-1</sup> s<sup>-1</sup> (Table 1). For comparison, this is approximately 3 times less than the OH + methanol rate coefficient and 10 times greater than for the OH + acetonitrile reaction.<sup>31</sup> With an average tropospheric concentration [OH]  $\sim 1 \times 10^6$  molecules cm<sup>-3</sup>, the HAN lifetime with respect to removal by OH is  $\sim$ 45 days. The uncertainty of up to  $\pm 2$  kJ mol<sup>-1</sup> in the reaction barrier heights implies a factor of  $\sim$ 2 uncertainty in the calculated rate coefficient and a similar uncertainty in the lifetime.

As noted in Section 3.1, decomposition of low partial-pressures of HAN to CH<sub>2</sub>O + HCN (R9) is thermodynamically favored. Prior computational analysis yielded a high barrier for direct dissociation with a slightly more favorable path via isomerization of HAN to HOCH<sub>2</sub>NC followed by dissociation of the isonitrile.<sup>41</sup> The latter step is the bottleneck for which we derive a barrier of 288 kJ mol<sup>-1</sup> relative to HAN. Therefore, (R9) is negligible in the atmosphere.

HAN is soluble in water  $^{42}$  and if dissolved in cloud aerosol, it will dissociate in solution, especially at high pH, on a time scale of hours. The rate-limiting step is reversible loss of  $\rm CN^-(aq)$  from  $\rm OCH_2CN^-(aq)$ . We speculate that the atmospheric lifetime with respect to this loss mechanism might be similar to the removal of other soluble compounds by cloud droplets, for which  $\sim 7$  days is recommended. In the context of astrochemistry within molecular clouds, it has been argued that dissociation and formation of HAN are heterogeneously catalyzed by water clusters or ice-coated grains.

We considered possible photolysis of HAN. The UV spectrum has not been reported in the literature, so we made configuration interaction calculations with single substitutions (CIS/aug-cc-pVTZ) to investigate the possibility of electronically excited states accessible by UV—visible absorption. This revealed an absence of transitions at wavelengths longer than 200 nm, so photolysis does not appear likely to be a rapid removal path for HAN in the troposphere. This is in accord with measured UV spectra of methanol and acetonitrile, 45 which indicate the hydroxy and nitrile groups not absorb above 200 nm. The implication of an average lifetime of around 7 days, and in the absence of clouds considerably longer, is that this component of smoke plumes could be transported long distances.

We now comment briefly on the formation and likely atmospheric fate of the HOCHCN radical and OCH2CN radical formed in the OH + HAN gas-phase reaction. The dominant channel (R1) leads to the formation of HOCHCN, an  $\alpha$ -hydroxyalkyl radical. Subsequent reaction with molecular oxygen is expected to rapidly form HO2 and the aldehyde HC(O)CN (formyl cyanide) through a mechanism involving the initial formation of a HOCH(OO)CN peroxy radical followed by H-transfer from HO- to OO- and elimination of HO<sub>2</sub>. 46 If the peroxy radical was stabilized, then reaction with NO to form the alkoxy species HOCH(O)CN followed by removal of the H atom from C-H through collision with a second O2 molecule could lead to the formation of HOC(O)CN, cyanoformic acid. Enthalpies of formation for both these nitrile products were derived via the working reactions (R6 and R7). There has been a past discrepancy between experimental<sup>47</sup> and computed<sup>48</sup> thermochemistry for

formyl cyanide, with  $\Delta_{\rm f}H_{298}$  proposed as 26  $\pm$  20 and 55 kJ  $\mathrm{mol}^{-1}$ , respectively. For formyl cyanide, we obtain  $\Delta_{\mathrm{f}}H_0$  and  $\Delta_{\rm f}H_{298}$  as 51.76 and 49.81 kJ mol<sup>-1</sup>, respectively, with an uncertainty of 1.4 kJ mol<sup>-1</sup> arising mainly from ZPVE. This supports the suggestion that  $\Delta_{\rm f}H_{298}({\rm HC(O)CN})$  should be raised to the top or beyond of its experimental range. We are not aware of prior thermochemistry for cyanoformic acid. The derived  $\Delta_t H_0$  and  $\Delta_t H_{298}$  are -199.16 and -204.01 kJ mol<sup>-1</sup>, respectively, with an uncertainty of 1.5 kJ mol<sup>-1</sup>. The minor channel (R2) yields OCH<sub>2</sub>CN, and we expect atmospheric O<sub>2</sub> to abstract an H atom to yield HC(O)CN. Thus, formyl cyanide is likely the dominant product formed in the atmospheric oxidation of HAN by the OH radical via both (R1) and (R2), with a predicted yield of ca. 90%. In turn, a possible environmental fate of HC(O)CN is hydrolysis to formic acid and HCN, which occurs readily with water adsorbed on surfaces.8

The product of channel (R3) could undergo C-C fission to make CH2OH and HOCN radicals. Our derived thermochemistry indicates an endothermicity of 95 kJ mol<sup>-1</sup> for the decomposition of the reaction product and so at room temperature, with an assumed A factor of  $\sim 10^{15}$  s<sup>-1</sup>, this process might have a first-order rate coefficient on the order of 0.01 s<sup>-1</sup>. A competing atmospheric fate is formation of a peroxy radical by addition of O2 to the radical center on the N atom, with an effective atmospheric first-order rate coefficient of the order of 10<sup>7</sup> s<sup>-1</sup>, likely followed by O atom abstraction by reaction with NO. For analogous perfluoronitrile/OH adducts, subsequent steps involving H-shifts or H-transfers have been proposed, leading to nitrosocarbonyl compounds, NO and, following reaction with a second NO molecule,  $N_2O.^{49,50}$  There is insufficient information about analogs of channel (R3) to be definitive about the multiple pathways available for subsequent chemistry of the radical adduct, and direct experimental measurements are desirable.

# 4. SUMMARY

Our calculations indicate that, like for methanol, the dominant path for OH reaction with hydroxyacetylnitrile is abstraction of H from C–H bonds (see Table 1). Despite the reduced C–H bond strength in HAN, and because both the OH and CN groups provide opportunities for favorable dipole or hydrogen bond interactions that can stabilize the TSs, the total reactivity is about 3 times less than methanol. This reflects the lowered entropy in the TSs also caused by these attractive forces. An estimated atmospheric lifetime with respect to OH chemistry is 45 days, and we note that heterogeneous loss on water aerosol could be significant. The dominant product of OH reaction is formyl cyanide with ca. 90% yield, which may ultimately be a source of HCN.

# ASSOCIATED CONTENT

# Supporting Information

The Supporting Information is available free of charge at https://pubs.acs.org/doi/10.1021/acsearthspace-chem.4c00176.

Computed geometries of stationary points on the OH + HOCH<sub>2</sub>CN potential energy surface (Table S1), harmonic and fundamental vibrational frequencies (Table S2), computed energies (Table S3) and potentials for low-barrier torsions (Figure S1) (PDF)

#### AUTHOR INFORMATION

# **Corresponding Author**

Paul Marshall — Chemical Sciences Laboratory, National Oceanic and Atmospheric Administration, Boulder, Colorado 80305-3327, United States; Cooperative Institute for Research in Environmental Sciences, University of Colorado, Boulder, Colorado 80309, United States; Department of Chemistry and Center for Advanced Scientific Modeling and Computing, University of North Texas, Denton, Texas 76203-5017, United States; orcid.org/0000-0002-8181-983X; Email: paul.marshall@unt.edu

## **Author**

James B. Burkholder — Chemical Sciences Laboratory, National Oceanic and Atmospheric Administration, Boulder, Colorado 80305-3327, United States; Ocid.org/0000-0001-9532-6246

Complete contact information is available at: https://pubs.acs.org/10.1021/acsearthspacechem.4c00176

### **Notes**

The authors declare no competing financial interest.

# ACKNOWLEDGMENTS

This work was supported in part by the NOAA Climate Program Office's Atmospheric Chemistry, Carbon Cycle and Climate Programs, and NASA's Atmospheric Composition Program. P.M. thanks CIRES for support through its Cooperative Agreement with NOAA, NA17OAR4320101. Computing facilities were provided by NOAA High Performance Computing and Communications and by UNT (supported by NSF awards CHE-1531468 and OAC-2117247).

# REFERENCES

- (1) Crutzen, P. J.; Andreae, M. O. Biomass Burning in the Tropics: Impact on Atmospheric Chemistry and Biogeochemical Cycles. *Science* **1990**, 250, 1669–1678.
- (2) Roberts, J. M.; Stockwell, C. E.; Yokelson, R. J.; de Gouw, J.; Liu, Y.; Selimovic, V.; Koss, A. R.; Sekimoto, K.; Coggon, M. M.; Yuan, B.; Zarzana, K. J.; Brown, S. S.; Santin, C.; Doerr, S. H.; Warneke, C. The nitrogen budget of laboratory-simulated western US wildfires during the FIREX 2016 Fire Lab study. *Atmos. Chem. Phys.* **2020**, 20, 8807—8826
- (3) Finewax, Z.; Chattopadhyay, A.; Neuman, J. A.; Roberts, J. M.; Burkholder, J. B. The air we breathe: calibration of hydroxacetonitrile (HOCH<sub>2</sub>CN) and methyl isocyanate (CH<sub>3</sub>NCO) isomers using I<sup>-</sup> chemical ionization mass spectrometry (CIMS). *Atmos. Meas. Tech.* **2024**. .
- (4) Cazzoli, G.; Lister, D. G.; Mirri, A. M. Rotational Isomerism and Barriers to Internal Rotation in Hydroxyacetonitrile from Microwave Spectroscopy. *J. Chem. Soc., Faraday Trans.* 2 **1973**, 69 (69), 569–578.
- (5) Dalbouha, S.; Domínguez-Gómez, R. M.; Senent, M. L. Structural and Spectroscopic Characterization of Various Isotopologues of 2-Hydroxyacetonitrile using Highly Correlated ab initio Methods. *Eur. Phys. J. D* **2017**, *71*, 161.
- (6) Margulès, L.; McGuire, B. A.; Senent, M. L.; Motiyenko, R. A.; Remijan, A.; Guillemin, J. C. Submillimeter spectra of 2-hydroxyacetonitrile (glyconitrile; HOCH<sub>2</sub>CN) and its searches in GBT PRIMOS observations of Sgr B2(N). *Astron. Astrophys.* **2017**, 601, A50.
- (7) Tonolo, F.; Lupi, J.; Puzzarini, C.; Barone, V. The Quest for a Plausible Formation Route of Formyl Cyanide in the Interstellar

- Medium: a State-of-the-Art Quantum-Chemical and Kinetic Approach. Astrophys. J. 2020, 900, 85.
- (8) Lewis-Bevan, W.; Gaston, R. D.; Tyrrell, J.; Stork, W. D.; Salmon, G. L. Formyl Cyanide: A Stable Species. Experimental and Theoretical Studies. *J. Am. Chem. Soc.* **1992**, *114*, 1933–1938.
- (9) Remijan, A. J.; Hollis, J. M.; Lovas, F. J.; Stork, W. D.; Jewell, P. R.; Meier, D. S. Detection of Interstellar Cyanoformaldehyde (CNCHO). *Astrophys. J.* **2008**, *675*, L85–L88.
- (10) Zeng, S.; Quénard, D.; Jiménez-Serra, I.; Martín-Pintado, J.; Rivilla, V. M.; Testi, L.; Martín-Doménech, R. First Detection of the Pre-Biotic Molecule Glycolonitrile (HOCH<sub>2</sub>CN) in the Interstellar Medium. *Mon. Not. R. Astron. Soc.: Lett.* **2019**, 484, L43.
- (11) Zhao, G.; Quan, D.; Zhang, X.; Feng, G.; Zhou, J.; Li, D.; Meng, Q.; Chang, Q.; Yang, X.; He, M.; Ma, M.-S. Glycolonitrile (HOCH<sub>2</sub>CN) Chemistry in Star-forming Regions. *Astrophys. J., Suppl. Ser.* **2021**, 257, 26.
- (12) Grimme, S. Semiempirical hybrid density functional with perturbative second-order correlation. *J. Chem. Phys.* **2006**, *124*, 034108.
- (13) Grimme, S.; Antony, J.; Ehrlich, S.; Krieg, H. A consistent and accurate ab initio parametrization of density functional dispersion correction (DFT-D) for the 94 elements H-Pu. *J. Chem. Phys.* **2010**, 132, 154104.
- (14) Dunning, T. H., Jr Gaussian basis sets for use in correlated molecular calculations. I. The atoms boron through neon and hydrogen. J. Chem. Phys. 1989, 90, 1007–1023.
- (15) Elliott, S. N.; Moore, K. B., III; Copan, A. V.; Georgievskii, Y.; Keçeli, M.; Somers, K. P.; Ghosh, M. K.; Curran, H. J.; Klippenstein, S. J. Systematically derived thermodynamic properties for alkane oxidation. *Combust. Flame* **2023**, 257, 112487.
- (16) Johnson, R. D., III NIST Computational Chemistry Comparison and Benchmark Database, release 22 (National Institute of Standards and Technology) http://cccbdb.nist.gov (accessed October 2023).
- (17) Purvis, G. D., III; Bartlett, R. J. A full coupled-cluster singles and doubles model the inclusion of disconnected triples. *J. Chem. Phys.* **1982**, *76*, 1910–1918.
- (18) Lee, T. J.; Taylor, P. R. A diagnostic for determining the quality of single-reference electron correlation methods. *Int. J. Quantum Chem.* **1989**, 36, 199–207.
- (19) Neese, F.; Valeev, E. F. Revisiting the Atomic Natural Orbital Approach for Basis Sets: Robust Systematic Basis Sets for Explicitly Correlated and Conventional Correlated ab initio Methods? *J. Chem. Theory Comput.* **2011**, *7*, 33–43.
- (20) Frisch, M. J.; Trucks, G. W.; Schlegel, H. B.; Scuseria, G. E.; Robb, M. A.; Cheeseman, J. R.; Scalmani, G.; Barone, V.; Petersson, G. A.; Nakatsuji, H.; Li, X.; Caricato, M.; Marenich, A. V.; Bloino, J.; Janesko, B. G.; Gomperts, R.; Mennucci, B.; Hratchian, H. P.; Ortiz, J. V.; Izmaylov, A. F.; Sonnenberg, J. L.; Williams; Ding, F.; Lipparini, F.; Egidi, F.; Goings, J.; Peng, B.; Petrone, A.; Henderson, T.; Ranasinghe, D.; Zakrzewski, V. G.; Gao, J.; Rega, N.; Zheng, G.; Liang, W.; Hada, M.; Ehara, M.; Toyota, K.; Fukuda, R.; Hasegawa, J.; Ishida, M.; Nakajima, T.; Honda, Y.; Kitao, O.; Nakai, H.; Vreven, T.; Throssell, K.; Montgomery, J. A.; Peralta, J. E.; Ogliaro, F.; Bearpark, M. J.; Heyd, J. J.; Brothers, E. N.; Kudin, K. N.; Staroverov, V. N.; Keith, T. A.; Kobayashi, R.; Normand, J.; Raghavachari, K.; Rendell, A. P.; Burant, J. C.; Iyengar, S. S.; Tomasi, J.; Cossi, M.; Millam, J. M.; Klene, M.; Adamo, C.; Cammi, R.; Ochterski, J. W.; Martin, R. L.; Morokuma, K.; Farkas, O.; Foresman, J. B.; Fox, D. J. Gaussian 16. Rev. A.03: Wallingford, CT, 2016.
- (21) Kállay, M.; Nagy, P. R.; Mester, D.; Rolik, Z.; Samu, G.; Csontos, J.; Csóka, J.; Szabó, P. B.; Gyevi-Nagy, L.; Hégely, B.; Ladjánszki, I.; Szegedy, L.; Ladóczki, B.; Petrov, K.; Farkas, M.; Mezei, P. D.; Ganyecz, A. The MRCC program system: Accurate quantum chemistry from water to proteins. J. Chem. Phys. 2020, 152, 074107. (22) Stanton, J. F.; Gauss, J.; Cheng, L.; Harding, M. E.; Matthews, D. A.; Szalay, P. G.; Auer, A. A.; Bartlett, R. J.; Benedikt, U.; Berger, C.; Bernholdt, D. E.; Bomble, Y. J.; Christiansen, O.; Engel, F.; Faber,

R.; Heckert, M.; Heun, O.; Huber, C.; Jagau, T.-C.; Jonsson, D.; Jusélius, J.; Klein, K.; Lauderdale, W. J.; Lipparini, F.; Metzroth, T.;

- Mück, L. A.; O'Neill, D. P.; Price, D. R.; Prochnow, E.; Puzzarini, C.; Ruud, K.; Schiffmann, F.; Schwalbach, W.; Simmons, C.; Stopkowicz, S.; Tajti, A.; Vázquez, J.; Wang, F.; Watts, J. D. *Cfour version 2.1*, 2019. http://www.cfour.de.
- (23) Georgievskii, Y.; Klippenstein, S. J. Strange Kinetics of the  $C_2H_6$  + CN Reaction Explained. *J. Phys. Chem. A* **2007**, *111*, 3802–3811.
- (24) Wheeler, S. E.; Houk, K. N.; Schleyer, P. v. R.; Allen, W. D. A Hierarchy of Homodesmotic Reactions for Thermochemistry. *J. Am. Chem. Soc.* **2009**, *131*, 2547–2560.
- (25) Ruscic, B.; Bross, D. H. *Active Thermochemical Tables*. version 1.130; Argonne National Laboratory. accessed November, 2023. http://atct.anl.gov.
- (26) Chase, M. W., Jr NIST-JANAF Thermochemical Tables, 4th ed.; American Chemical Society and the American Institute of Physics: Woodbury, NY, 1998.
- (27) Truhlar, D. G.; Garrett, B. C. Variational Transition-State Theory. Acc. Chem. Res. 1980, 13, 440-448.
- (28) Barker, J. R.; Nguyen, T. L.; Stanton, J. F.; Aieta, C.; Ceotto, M.; Gabas, F.; Kumar, T. J. D.; Li, C. G. L.; Lohr, L. L.; Maranzana, A.; Ortiz, N. F.; Preses, J. M.; Simmie, J. M.; Sonk, J. A.; Stimac, P. J. *MultiWell-2023.1 Software Suite*; University of Michigan: Ann Arbor, MI, 2023. https://multiwell.engin.umich.edu.
- (29) Coote, M. L.; Collins, M. A.; Radom, L. Calculation of accurate imaginary frequencies and tunnelling coefficients for hydrogen abstraction reactions using IRCmax. *Mol. Phys.* **2003**, *101*, 1329–1338.
- (30) Troe, J. Predictive possibilities of unimolecular rate theory. J. Phys. Chem. 1979, 83, 114–126.
- (31) Burkholder, J. B.; Sander, S. P.; Abbatt, J.; Barker, J. R.; Cappa, C.; Crounse, J. D.; Dibble, T. S.; Huie, R. E.; Kolb, C. E.; Kurylo, M. J.; Orkin, V. L.; Percival, C. J.; Wilmouth, D. M.; Wine, P. H. Chemical Kinetics and Photochemical Data for Use in Atmospheric Studies. Evaluation No. 19. Publication 19–5; NASA/JPL: Pasadena, CA, 2019. http://jpldataeval.jpl.nasa.gov.
- (32) Chrostowska, A.; Darrigan, C.; Dargelos, A.; Benidar, A.; Guillemin, J.-C. The Electronic Structure of some Cyanohydrins A Spectroscopically Under-Investigated Family of Compounds. *Chem-PhysChem* **2015**, *16*, 3660–3671.
- (33) Mielke, Z.; Hawkins, M.; Andrews, L. Matrix Reactions of Oxygen Atoms with CH<sub>3</sub>CN. Infrared Spectra of HOCH<sub>2</sub>CN and CH<sub>3</sub>CNO. *J. Phys. Chem.* **1989**, 93, 558.
- (34) Danger, G.; Duvernay, F.; Theulé, P.; Borget, F.; Guillemin, J.-C.; Chiavassa, T. Hydroxyacetonitrile (HOCH<sub>2</sub>CN) as a precursor for formylcyanide (CHOCN), ketenimine (CH<sub>2</sub>CNH), and cyanogen (NCCN) in astrophysical conditions. *Astron. Astrophys.* **2013**, 549, A93.
- (35) Rienstra-Kiracofe, J. C.; Allen, W. D.; Schaefer, H. F., III The  $C_2H_5+O_2$  Reaction Mechanism: High-Level ab Initio Characterizations. *J. Phys. Chem. A* **2000**, *104*, 9823–9840.
- (36) Heard, D. E. Rapid Acceleration of Hydrogen Atom Abstraction Reactions of OH at Very Low Temperatures through Weakly Bound Complexes and Tunneling. *Acc. Chem. Res.* **2018**, *51*, 2620–2627.
- (37) Forst, W. Temperature-dependent A factor in thermal unimolecular reactions. *J. Phys. Chem.* **1979**, *83*, 100–108.
- (38) Gao, L. G.; Zheng, J.; Fernández-Ramos, A.; Truhlar, D. G.; Xu, X. Kinetics of the Methanol Reaction with OH at Interstellar, Atmospheric, and Combustion Temperatures. *J. Am. Chem. Soc.* **2018**, 140, 2906–2918.
- (39) Nguyen, T. L.; Ruscic, B.; Stanton, J. F. A master equation simulation for the OH + CH<sub>3</sub>OH reaction. *J. Chem. Phys.* **2019**, *150*, 084105.
- (40) Georgievskii, Y.; Klippenstein, S. J. Long-range transition state theory. *J. Chem. Phys.* **2005**, *122*, 194103.
- (41) Woon, D. E. Ab Initio Quantum Chemical Studies of Reactions in Astrophysical Ices 2. Reactions in H<sub>2</sub>CO/HCN/HNC/H<sub>2</sub>O Ices. *Icarus* **2001**, *149*, 277–284.

- (42) Lide, D. R. CRC Handbook of Chemistry and Physics, 82nd ed.; CRC Press: Boca Raton, 2001–2002.
- (43) Schlesinger, G.; Miller, S. L. Equilibrium and Kinetics of Glyconitrile Formation in Aqueous Solution. *J. Am. Chem. Soc.* **1973**, 95, 3729–3735.
- (44) Annex—Scientific Assessment of Ozone Depletion: 2022, GAW Report No. 278. World Meteorological Organization: Geneva, 2022, https://csl.noaa.gov/assessments/ozone/2022/downloads/Annex\_2022OzoneAssessment.pdf.
- (45) Keller-Rudek, H.; Moortgat, G. K.; Sander, R.; Sörensen, R. The MPI-Mainz UV/VIS Spectral Atlas of Gaseous Molecules of Atmospheric Interest. *Earth Syst. Sci. Data* **2013**, *5*, 365–373.
- (46) Hermans, I.; Müller, J. F.; Nguyen, T. L.; Jacobs, P. A.; Peeters, J. Kinetics of α-Hydroxy-alkylperoxyl Radicals in Oxidation Processes. HO<sub>2</sub>•-Initiated Oxidation of Ketones/Aldehydes near the Tropopause. *J. Phys. Chem. A* **2005**, *109*, 4303–4311.
- (47) Born, M.; Ingemann, S.; Nibbering, N. M. M. Experimental Determination of the Enthalpies of Formation of Formyl Cyanide and Thioformyl Cyanide in the Gas Phase. *J. Phys. Chem.* **1996**, *100*, 17662–17669.
- (48) Nguyen, T. L.; Nguyen, M. T. On the Heats of Formation of Formyl Cyanide and Thioformyl Cyanide. *J. Chem. Phys.* **1999**, *110*, 684–686.
- (49) Guo, Q.; Chen, L.; Kutsuna, S.; Quan, H.; Mizukado, J. Atmospheric chemistry of perfluoronitriles: Environmental impact and experimental evidence related to  $N_2O$  and NO formation. *Atmos. Environ.* **2019**, 198, 175–182.
- (50) Sulbaek Andersen, M. P.; Ohide, J.; Sølling, T. I.; Nielsen, O. J. Atmospheric chemistry of CF<sub>3</sub>CN: kinetics and products of reaction with OH radicals, Cl atoms and O<sub>3</sub>. *Phys. Chem. Chem. Phys.* **2022**, 24, 2638–2645.